A physics-, SCADA-based remaining useful life calculation approach for wind turbine drivetrains

Diederik van Binsbergen[1], **Marcelo Nesci Soares**[2], **Eilif Pedersen**[1], **Amir R. Nejad**[1]

[1] Department of Marine Technology, Norwegian University of Science and Technology (NTNU), Otto Nielsens veg 10, 7052 Trondheim, Norway
[2] Federal Center of Technological Education "Celso Suckow da Fonseca" (CEFET/RJ), Rio de Janeiro, Brazil

E-mail: dirk.w.van.binsbergen@ntnu.no, marcelo.soares@cefet-rj.br

Abstract. This paper describes the development of a physics-, SCADA-based model able to predict the expected lifetime for wind turbine drivetrains. A real-time coupled torsional gearbox-generator model is developed using the bond graph approach in the software 20SIM. The model uses SCADA data with a sampling frequency of one hertz to impose a load reference on the wind turbine for the simulation model. From the SCADA measurements, rotor torque is estimated and used as input load to the wind turbine rotor, while generator speed is used as reference in the control loop for maximum power point tracking. Shaft torsion is used to predict high-speed shaft radial and axial bearing loads from static equilibrium. The load amplitude and the number of stress cycles are calculated using the load duration distribution method and damage is calculated using Miner's rule. Expected lifetime is predicted by linear extrapolation of the accumulated fatigue damage to the fatigue limit. Results show that the model can capture the torsional and electrical dynamics and that the model results agree with the reference input. The radial bearing loads match well with literature where additional sensors are used to determine the loads.

1. Introduction

Wind turbine (WT) condition monitoring is becoming increasingly more important due to the increased cost associated with offshore repairs. WTs have been moving further offshore, causing longer downtime and higher repair costs. Stehly et al. [1] report that the operational expenditure (OpEx) for land-based WTs can range between 32 and 54 $\$/kW/year$, while for offshore wind this can range between 62 and 186 $\$/kW/year$. Faulstisch et al. [2] mention that generator and gearbox failures cause long downtime and result in high repair costs. Furthermore, Nejad et al. [3] report that generator and gearbox reliability improvement and condition monitoring development are especially important. Advancing from corrective to predictive maintenance strategies can be used for remaining useful life prediction and end-of-life decision-making. This will subsequently result in a reduction of the OpEx and the levelized cost of energy (LCOE). Condition monitoring with the use of turbine supervisory control and data acquisition (SCADA) and condition monitoring systems (CMS) can be used to actively track system properties and can provide early detection of faults in WTs.

Condition monitoring can be subdivided into data-driven, physics-based and hybrid methods. The potential of physics-based models is large but these models require additional knowledge

on the WT [4; 5], such as modal parameters [6], which are rarely available to WT operators. Condition monitoring, both data-driven and physics-based, can require additional sensors. This increases the cost related to condition monitoring and requires installation before or after the operational start of the WT and can result in additional downtime. Monitoring properties based on SCADA measurements is cost-effective since sensors are already installed and can be implemented directly. Moreover, with historical SCADA data available, the WT status can be easily exploited since the operational start of the WT. This does not apply when a CMS is added after the operational start of the WT.

In previous literature, coupled gearbox-generator models have been created [7–9] based on simulation data, but not based on SCADA measurements. Gear and bearing fatigue life calculations have been done based on time domain simulations [10–12]. In Gray and Watson [5] SCADA measurements are used to estimate torque from electrical power and the shaft rotational speed to further model bearing loads and damage. Here, the torsional dynamics of the drivetrain are not considered. Remigius and Natajaran [13] show that rotor torque can be estimated from SCADA data using an inverse approach. They modeled the drivetrain as a two degree of freedom (DOF) torsional model, consisting of two bodies with inertia and a shaft modeled as a viscously damped torsional spring and a gearbox ratio to adjust the torsional load and displacement between the low-speed shaft (LSS) and high-speed shaft (HSS). The state-of-the-art on physics-, SCADA-based models for WT condition monitoring is therefore limited, while Helsen [14] mentions that the use of physical simulation models can contribute significantly to the remaining useful life assessment of the asset. Liu et al. [15] summarized WT bearing failure modes and mentioned that fatigue fracture, among other failure modes, can occur for all bearings in the WT. Increasing the accuracy of load calculations based on SCADA measurements will influence the high cycle fatigue assessment. Thus the need for high accuracy physical models is of significant importance for future prognostics.

The objective of this work is to develop a real-time physics-, SCADA-based model able to:

(i) calculate torsional loads across the drivetrain and electrical dynamics of the generator (voltages and currents).

(ii) predict remaining useful life on drivetrain and generator components.

The scope of this work mainly focuses on the development and validation of the coupled gearbox and generator model and will be used to determine bearing load responses and deterministic high cycle fatigue damage on the HSS.

In future work, the model can be used in a digital twin framework, where system parameter estimation due to degradation can be included in combination with stochastic degradation models, as shown in Moghadam et al. [6]. The model can be used for fault sensitivity analysis between the mechanical and electrical components of the WT.

The rest of the paper is organized as follows: In section 2 the coupled gearbox-generator, load estimation and damage accumulation models are presented. Then, in section 3 the model is validated using SCADA data and previous literature followed by results on the deterministic damage and remaining useful life results for high cycle fatigue. Finally, in section 4 concluding remarks are made and future work will be elaborated on.

2. Methodology

The bond graph (BG) [16] approach is used to construct the real-time coupled torsional gearbox-generator model of the WT since it is well suited for complex multi-domain systems. SCADA measurements with a sampling frequency of one hertz (Hz) are used to impose a load reference on the WT for the simulation model. Shaft torsion is calculated across the drivetrain and voltages and currents of the generator are calculated. Radial and axial bearing loads are calculated on the HSS using static equilibrium. Stress cycles are counted using the load duration distribution

(LDD) [17; 18] method and Miner's rule [19] is used to model damage accumulation. Expected lifetime is predicted based on linear extrapolation. Radial bearing loads on the HSS are compared to the results of Guo and Keller [20], where strain gauge measurements are used to predict the bending moment on the HSS in order to solve static equilibrium. The generator model is validated using the available wound rotor induction machine in Matlab/Simulink [21].

In subsection 2.1 literature and measurement data relevant to the development of the case study model are mentioned. In subsection 2.2 it is explained how the load reference on the rotor side is calculated using SCADA data. In subsection 2.3 the bond graph approach is further introduced and in subsection 2.4 the developed model is discussed. Due to the stiff nature of the system, subsection 2.5 substantiates the solver choice. Bearing load estimation and fatigue damage accumulation are discussed in subsection 2.6 and 2.7 respectively.

2.1. Case study data

An approach for developing a physics-based model based on data extracted from measurements was introduced by van Binsbergen et al. [22]. The considered case consists of a 1.5MW doubly-fed induction generator (DFIG) WT and its information is available in NREL technical reports [23–25] and in Guo and Keller [20]. Experimental data is provided by the National Renewable Energy Laboratory (NREL) [26] and is publicly available. Further information on the gearbox topology and model parameters can be found in van Binsbergen et al. [22].

2.2. Load reference

The load reference for the model is determined from SCADA measurements, which are denoted by *. The SCADA power production (P^*), rotor speed (Ω_r^*) and generator speed (Ω_g^*) are used to determine the input references of the 20SIM [27] model. Rotor torque (T_r) is used as load reference to the wind turbine rotor, while Ω_g^* is used as reference in the control loop for maximum power point tracking (MPPT). The rotor torque is determined using Equation 1, which is derived from the equations of motion (EOM) for a torsional 2 DOF drivetrain system:

$$T_r = J_r\dot{\Omega}_r^* + N(T_g + J_g\dot{\Omega}_g^*), \tag{1}$$

where J_r and J_g represent the rotor and generator inertia respectively. N is the inverse of the gearbox ratio and $\dot{\Omega}_r^*$ and $\dot{\Omega}_g^*$ are the rotor and generator shaft acceleration respectively. The generator torque (T_g) is calculated from $P^* = T_g\Omega_g^*$. This is a valid assumption when power is measured either before or after the converter since the converter has a limited influence on the system dynamics. A Butterworth filter is applied on the rotor torque input and the control reference with a cut-off frequency of $0.25Hz$. This assumption makes the results smoother and has limited consequences on the available dynamics in the data since the Nyquist frequency is $0.5Hz$. Moreover, the power electronic converter has been considered ideal in this model and therefore the output rotor voltages to control the generator are purely sinusoidal.

2.3. Bond graph approach

The BG modeling approach is used to construct the coupled gearbox-generator model. BGs are a graphical notation of energy flow in physical systems where half arrows, also called power bonds, represent the flow of energy between systems or elements. 1- and 0-junctions represent the distribution of energy, with equal flow and effort respectively, while I-C- and R-elements represent energy storage (flow storage and effort storage respectively) and energy dissipation. BGs automatically provide the model equations in state-space form which can be solved through a variety of integration methods. A thorough description of BG modeling can be found in Karnopp et al. [16].

2.4. Wind turbine model

The coupled WT gearbox-generator model is implemented in 20SIM [27]. Figure 1 shows an overview of the model. The **SCADA** submodel contains the reference power production, reference rotor speed and reference generator speed for the **LoadReference** and **Control** submodel. In the **LoadReference** submodel, the rotor torque is calculated from SCADA measurements and is applied on the rotor side of the **Gearbox** submodel. The **Gearbox** submodel is represented as a 7 DOF system and receives the rotor torque and electromagnetic torque (T_e) as input from the **LoadReference** and **Generator** submodel respectively and outputs the mechanical generator speed (Ω_g) towards the generator and controller. Here it is assumed that the electromagnetic torque is the same as the generator torque. The **Generator** submodel represents the generator as a DFIG, connected to a 575V/60Hz grid, and the **Control** submodel represents the controller for the DFIG. First, the optimal speed reference from SCADA data is applied in the generator speed control loop. Hence, the control is following the MPPT power curve of the real wind turbine. Furthermore, the electromagnetic torque and rotor-side currents are necessary as input to the control loop in order to control the rotor-side voltages of the generator. From the **Gearbox** submodel, the HSS torque (T_{hss}) and HSS rotational speed (Ω_{hss}) are extracted and the gear teeth load (F_t) is calculated from the HSS torque and pinion base radius (R_b): $F_t = \frac{T_{hss}}{R_b}$. The axial load ($F_a$) can then be calculated using the helix angle of the gear-pinion stage, which is further elaborated in subsection 2.6. In the **LoadEstimation** submodel, the radial bearing loads on the HSS are calculated from static equilibrium. The radial bearing loads are compared to Guo and Keller [20], which uses strain gauge measurements to predict the bending moment on a specific place of the shaft to solve static equilibrium on the HSS. In the **Damage** submodels, damage accumulation is modeled for the rotor side radial bearing (FRS), generator side radial bearing (FGS) and the 4 point contact ball bearing (4PCBB). The LDD [17; 18] method is used to count the stress cycles and the Miner's rule [19] is used to calculate accumulated damage. Expected lifetime is predicted by linear extrapolation of the accumulated fatigue damage to the fatigue damage limit.

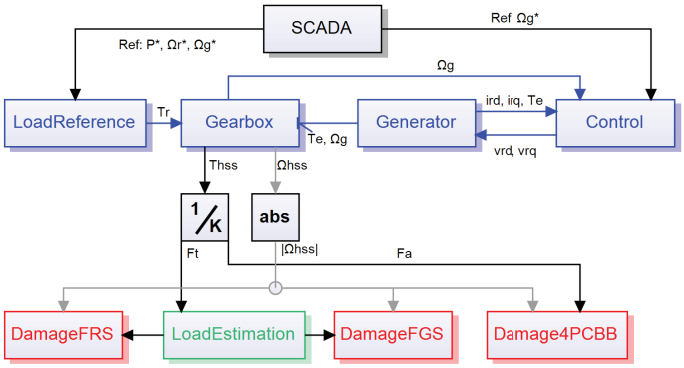

Figure 1. Case study model overview: Coupled gearbox-generator model including load reference and controller in blue, load estimation model in green and fatigue damage accumulation model in red.

2.4.1. Gearbox model: The WT drivetrain is modeled as a lumped parameter model with 7 torsional DOF. Gear meshing is modeled as rigid, while shafts are modeled as flexible beams. The shaft rotational stiffness (K) is determined geometrically, assuming an ideal cylinder and constant E-modulus, for each shaft and the equivalent stiffness is equal to the first torsional natural frequency of the drivetrain for the given rotor and generator inertia.

The EOM are derived using the Lagrange-Hamiltonian [28] method and are represented with an IC-element [16; 29]. The torque on each inertia element and the rotational speed of each inertia element is found by solving Equation 2 and 3 respectively.

$$\boldsymbol{e} \equiv \dot{\boldsymbol{p}} = \frac{\delta T}{\boldsymbol{\delta q}} - \frac{\delta V}{\boldsymbol{\delta q}} + \boldsymbol{E} = \boldsymbol{e'} + \boldsymbol{E}, \tag{2}$$

$$\boldsymbol{f} \equiv \dot{\boldsymbol{q}} = \boldsymbol{M}^{-1}\boldsymbol{p}, \tag{3}$$

where $\mathbf{e}$ and $\mathbf{f}$ represent the effort and flow respectively, $\mathbf{p}$ represents the generalized momentum and $\mathbf{q}$ represents the generalized coordinate. T and V are the kinetic and potential energy respectively and $\mathbf{M}$ is the mass matrix. $\mathbf{e}'$ contains all effort terms dependent on generalized coordinates and $\mathbf{E}$ contains the external effort sources.

$$\boldsymbol{e'} = -\begin{bmatrix} K_{lss}(\theta_r - \theta_{gs,1}) \\ K_{lss}(\theta_{gs,1} - \theta_r) - K_{iss}(\theta_{gs,2} - n_1 n_2 \theta_{gs,1}) \\ K_{iss}(\theta_{gs,2} - n_1 n_2 \theta_{gs,1}) - K_{iss,hss}(\theta_{gs,3} - n_3 \theta_{gs,2}) \\ K_{iss,hss}(\theta_{gs,3} - n_3 \theta_{gs,2}) - K_{hss}(\theta_{bd} - n_4 \theta_{gs,3}) \\ K_{hss}(\theta_{bd} - n_4 \theta_{gs,3}) - K_{bd,c}(\theta_c - \theta_{bd}) \\ K_{bd,c}(\theta_c - \theta_{bd}) - K_{c,gs}(\theta_g - \theta_c) \\ K_{c,gs}(\theta_g - \theta_c) \end{bmatrix}, \boldsymbol{E} = \begin{bmatrix} T_r \\ 0 \\ 0 \\ 0 \\ 0 \\ 0 \\ -T_g \end{bmatrix} \tag{4}$$

$\mathbf{e}'$ represents the stiffness torque and can be seen in Equation 4. $\mathbf{e}'$ is dependent on the generalized coordinate of the shaft position (θ) and K. Subscript $gs, 1$, $gs, 2$ and $gs, 3$ are abbreviations for gear stage 1, 2 and 3 respectively. Subscript bd and c represent the brake disk and the coupling respectively. Subscript n represents gear ratios of the gearbox, where n_1, n_2, n_3 and n_4 stand for the carrier-planet, planet-sun, gear-pinion stage 1 and gear-pinion stage 2 ratios respectively. ISS and GS are abbreviations for intermediate-speed shaft and generator shaft respectively. Damping is not considered since this method is energy conservative. $\mathbf{E}$ is the external torque on the gearbox, T_r and T_g.

$$\boldsymbol{M} = \begin{bmatrix} J_r & 0 & 0 & 0 & 0 & 0 & 0 \\ 0 & 3n_1^2 J_{pl} + n_1^2 n_2^2 J_{sun} & 0 & 0 & 0 & 0 & 0 \\ 0 & 0 & n_3^2 J_{pin,1} + J_{gear,1} & 0 & 0 & 0 & 0 \\ 0 & 0 & 0 & n_4^2 J_{pin,2} + J_{gear,2} & 0 & 0 & 0 \\ 0 & 0 & 0 & 0 & J_{bd} & 0 & 0 \\ 0 & 0 & 0 & 0 & 0 & J_c & 0 \\ 0 & 0 & 0 & 0 & 0 & 0 & J_g \end{bmatrix} \tag{5}$$

Mass matrix $\mathbf{M}$ is independent of any generalized coordinates or momenta and is shown in Equation 5. J is the moment of inertia around the axis of rotation of the rigid body. Subscript pl and pin are abbreviations for planet and pinion respectively. Figure 2 shows the **Gearbox** submodel. Equation 2 and 3 are solved in the IC-element without the external torque, $\mathbf{E}$. $\mathbf{E}$ is provided to the 1-junction from the left-hand and right-hand multibonds. T_r is provided as signal from the **LoadReference** submodel and converted to a [7x1] bond using the modulated effort source, **MSe**. Similarly, T_g is provided by the **Generator** submodel as [1x1] bond and is converted to a [7x1] bond using a transformer, **TF**. The generator speed (Ω_g) is then used in the control structure of the DFIG.

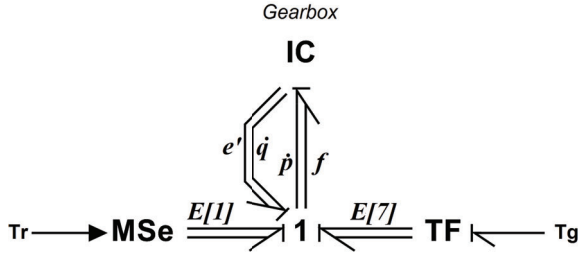

Figure 2. Case study: bond graph gearbox submodel.

2.4.2. Generator model and control structure: The equivalent circuit of the DFIG model [30; 31] can be seen in Figure 3. Subscript s and r indicate that the circuit elements are part of the stator-and rotor-side respectively. Subscript d and q indicate that the circuit elements are part of the direct and quadrature frame respectively. L_M, L_{lr} and L_{ls} are the magnetization, rotor and stator inductances respectively and R, λ, v and i are resistance, flux linkage, voltage and current respectively. ω is the angular velocity.

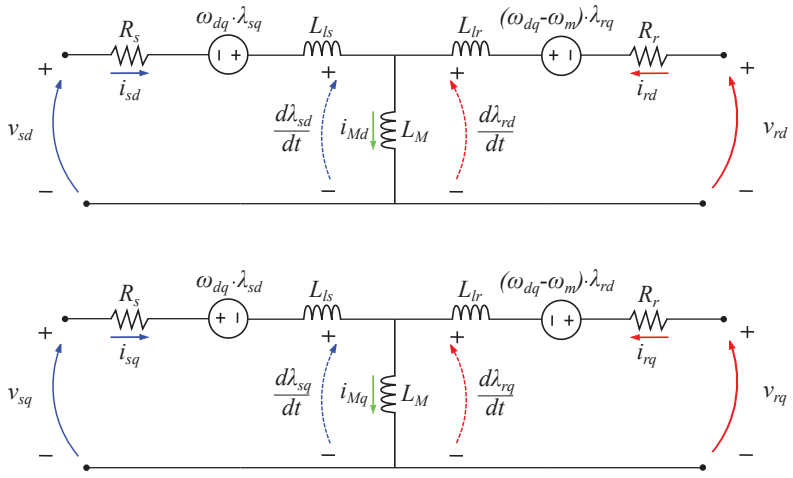

Figure 3. Equivalent circuit of a DFIG in dq frame.

Electromagnetic torque (T_e) is calculated using Equation 6, which is obtained by the simplification of the total instantaneous active power equation of the DFIG in dq frame.

$$T_e = \frac{3}{2}\frac{L_M}{L_s} P_p \left(\lambda_{sq} i_{rd} - \lambda_{sd} i_{rq}\right), \qquad L_s = L_M + L_{ls}, \qquad P_p : \#\text{ pole pairs} \tag{6}$$

The DFIG model in Figure 4 is derived from the equivalent circuit of the DFIG model in Figure 3 and Equation 6. In red the rotor-side electrical bonds and signals are shown, while in blue the stator-side electrical bonds and signals are shown. At the top and bottom 1-junctions the rotor-side and stator-side voltages are calculated in direct-quadrature (dq) frame. In green the flux linkage signals are shown, which are calculated, together with the current, at the M-element by solving the inductance matrix in dq frame (L_{dq}) [32] and is given by Equation 7.

$$\begin{bmatrix}\lambda_{sd}\\ \lambda_{sq}\\ \lambda_{rd}\\ \lambda_{rq}\end{bmatrix} = \begin{bmatrix}\int_{t_0}^{t_1} v_{sd}\,dt\\ \int_{t_0}^{t_1} v_{sq}\,dt\\ \int_{t_0}^{t_1} v_{rd}\,dt\\ \int_{t_0}^{t_1} v_{rq}\,dt\end{bmatrix}, \begin{bmatrix}i_{sd}\\ i_{sq}\\ i_{rd}\\ i_{rq}\end{bmatrix} = L_{dq}^{-1}\begin{bmatrix}\lambda_{sd}\\ \lambda_{sq}\\ \lambda_{rd}\\ \lambda_{rq}\end{bmatrix}, L_{dq} = \begin{bmatrix} L_{ls}+L_M & 0 & L_M & 0\\ 0 & L_{ls}+L_M & 0 & L_M\\ L_M & 0 & L_{lr}+L_M & 0\\ 0 & L_M & 0 & L_{lr}+L_M\end{bmatrix} \quad (7)$$

In cyan the angular velocity signals are shown. The mechanical generator speed (Ω_g) is taken from the left-hand 1-junction and is used to calculate the electrical angular velocity (ω_m) of the rotor as follows: $\omega_m = P_p\Omega_g$. The electrical angular rotor velocity (ω_r) of the circuit is calculated as follows: $\omega_r = \omega_s - \omega_m$, where $\omega_s = 2\pi f_s$ and the stator frequency (f_s) is 60 Hz. ω_s is the electrical angular stator velocity of the circuit and is described as ω_{dq} in Figure 3. Gain K multiplies the stator flux linkages with constant $K = \frac{3}{2}\frac{L_M}{L_s}P_p$ to calculate the electrical torque, shown in the left-hand 1-junction with orange bonds and signals.

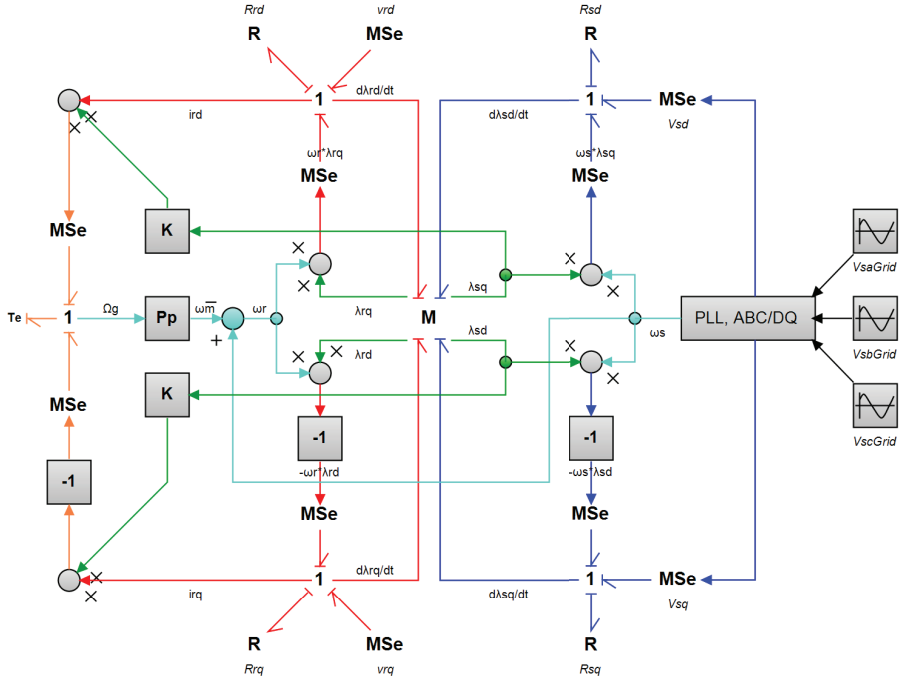

Figure 4. DFIG model.

The Park transform [33] and phase-locked loop (PLL) [34] are accommodated in the **PLL, ABC/DQ** submodel. The submodel performs the *abc* to *dq* transformation, as shown in Equation 8, and synchronizes the input phase to the grid phase.

$$\begin{bmatrix} x_d\\ x_q\end{bmatrix} = \frac{2}{3}\begin{bmatrix} \cos(\omega_{dq}t) & \cos(\omega_{dq}t-\frac{2\pi}{3}) & \cos(\omega_{dq}t+\frac{2\pi}{3})\\ -\sin(\omega_{dq}t) & -\sin(\omega_{dq}t-\frac{2\pi}{3}) & -\sin(\omega_{dq}t+\frac{2\pi}{3})\end{bmatrix}\begin{bmatrix} x_a\\ x_b\\ x_c\end{bmatrix} \quad (8)$$

The DFIG control [35; 36], shown in Figure 5, consists of PI-controllers in series that have the purpose to control the rotor-side voltages. The rotor-side direct voltage (v_{rd}), responsible for controlling the active power, uses the generator speed (Ω_g^*) from SCADA data as a reference to the speed control loop. The rotor-side quadrature voltage, responsible for controlling the

reactive power, is controlled by the rotor-side quadrature current, i^*_{rq}, where $i^*_{rq} = -\frac{v_{sd}}{\omega_s L_M}$. This quadrature current will provide a power factor closest to 1 for steady state conditions. Gain K_1, K_2 and K_3 are: $K_1 = \frac{L_M}{L_s}$, $K_2 = K_3 = L_r\sigma$, where $\sigma = \frac{L_r L_s - L_M^2}{L_r L_s}$ and $L_r = L_{lr} + L_M$.

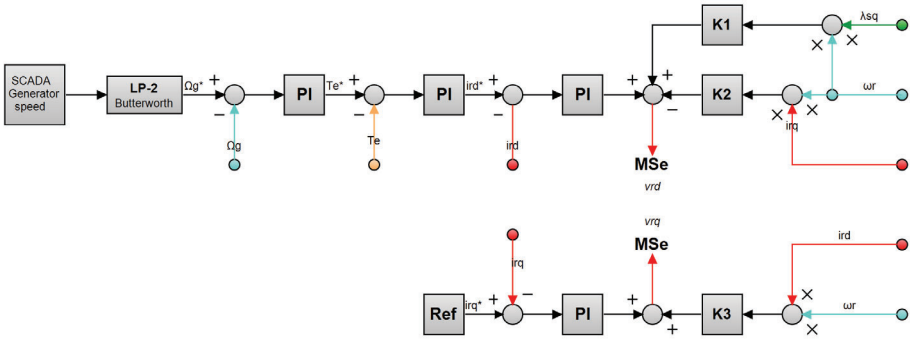

Figure 5. Control structure.

2.5. Integration method

The system is considered to be stiff due to the gearbox and the high ratio between mechanical inertia and electrical inductance. This will subsequently result in eigenvalues with a large difference in magnitude. Therefore the Vode Adams solver by Cohen and Hindmarsh [37] is used with an absolute and relative acceptable error of 10^{-10} for stability and accuracy considerations. The applied multistep method and iteration type are the backward differential formula (BDF) and Newton method respectively, suited best for stiff systems.

2.6. Bearing load estimation

Loads at bearings that support the pinion and the HSS are calculated. The case study WT shaft is supported by three bearings, mentioned in Guo and Keller [20]:

- NU2326: Radial roller bearing on the rotor-side of the pinion.
- NU232: Radial roller bearing on the generator-side of the pinion.
- QJ328: 4 point contact ball bearing (4PCBB) on the generator-side of the pinion.

SKF states that a 4PCBB in combination with radial roller bearings can carry axial loads only. It is assumed that the radial roller bearings only provide radial load support. Furthermore, it is assumed that the radial and axial loads on the bearings are primarily caused by the gear teeth load and the rotor side of the HSS is assumed to have a free end with zero moment. The radial bearing loads can then be calculated from static force and moment equilibrium in radial (Y and Z) direction. Further details on the equilibrium Equations can be found in Guo and Keller [20]. Radial bearing loads are compared with loads calculated in Guo and Keller [20]. Similarly, axial bearing loads can be calculated from static load equilibrium as follows: $F_a = F_t \tan(\beta)$, where β is the helix angle of gear-pinion stage 2. The helix angle of gear-pinion stage 2 is unknown. For further calculations a helix angle of 12° is assumed.

2.7. Damage accumulation

Accumulated fatigue damage is calculated for the rotor-side, generator-side and 4PCB bearing. First, the dynamic equivalent load (P_R) is calculated [38] as follows: $P_R = XF_r + YF_a$, where X and Y are bearing-specific load factors, given by manufacturers and F_r and F_a are the radial and axial load on the bearing.

The load amplitude and number of stress cycles are calculated using the LDD method as shown in Equation 9 [17; 18]. The total number of cycles to reach failure for a given load amplitude is calculated using the life Equation as shown in Equation 10 [38].

$$n_i = \frac{\Omega_i}{2\pi} dt, \tag{9}$$

where Ω_i is the rotational speed of the HSS for timestep i and dt is the solver timestep.

$$N_i = \left(\frac{C}{P_i}\right)^a, \tag{10}$$

where C is the basic dynamic load rating, a is a bearing geometric constant and P_i is the equivalent load for timestep i.

Accumulated fatigue damage is calculated using Miner's rule [19] as shown in Equation 11. $D = 1$ corresponds to a reliability of 90%. Load ratings and dynamic equivalent factors for each bearing are available at `SKF.com`. Expected lifetime is predicted by linear extrapolation of the accumulated fatigue damage to $D = 1$.

$$D = \sum_{i=1}^{k} \frac{n_i}{N_i} \tag{11}$$

3. Results and discussion

The results of the coupled gearbox-generator model are validated in subsection 3.1, where reference values are compared to model outputs and bearing load results are compared to Guo and Keller [20] for multiple measurement series. Deterministic damage accumulation results on the HSS bearings can be found in subsection 3.2.

3.1. Validation

The reference SCADA power production, rotor speed and generator speed are compared to the model results for multiple measurement series. Figure 6 shows these results in the top left-hand, top right-hand and centre left-hand plots respectively for one measurement series. DRC-uptower measurements [26] are used as load reference. A good agreement between the reference values and the model results is found when the turbine is producing power ($P_{el} > 0$). From Nejad et al. [39] it can be seen that short-term fatigue damage increases significantly with an increase in wind speed, thus it is assumed that high cycle fatigue for gears and bearings that provide radial load support is negligible below cut-in.

The rotor and generator torque are shown in the centre right-hand corner of Figure 6. A clear difference in torque load behaviour between the rotor and the generator can be seen, implying that the rotor and generator shaft acceleration should not be neglected when calculating either rotor or generator torque from the EOM. Bearing loads are compared to Guo and Keller [20] and results from one measurement series are shown at the bottom of Figure 6. It can be seen that loads calculated by the model match well with the work done by Guo and Keller [20]. This means that bearing loads on the case study HSS can be predicted without the additional need for strain gauges or other sensors when power is produced. Important to consider is that static equilibrium equations are solved both in this work and in Guo and Keller [20], assuming that the resultant of all forces acting on the shaft is equal to zero. Furthermore, loads due to other DOF are not considered. The axial load support by the 4PCBB is not shown in Figure 6 since no measurements from Guo and Keller [20] are available for this bearing. Also, the axial load magnitude is highly dependent on the helix angle of the gear-pinion set, which is assumed for the case study WT. The load magnitude is used for further damage calculations in subsection 3.2.

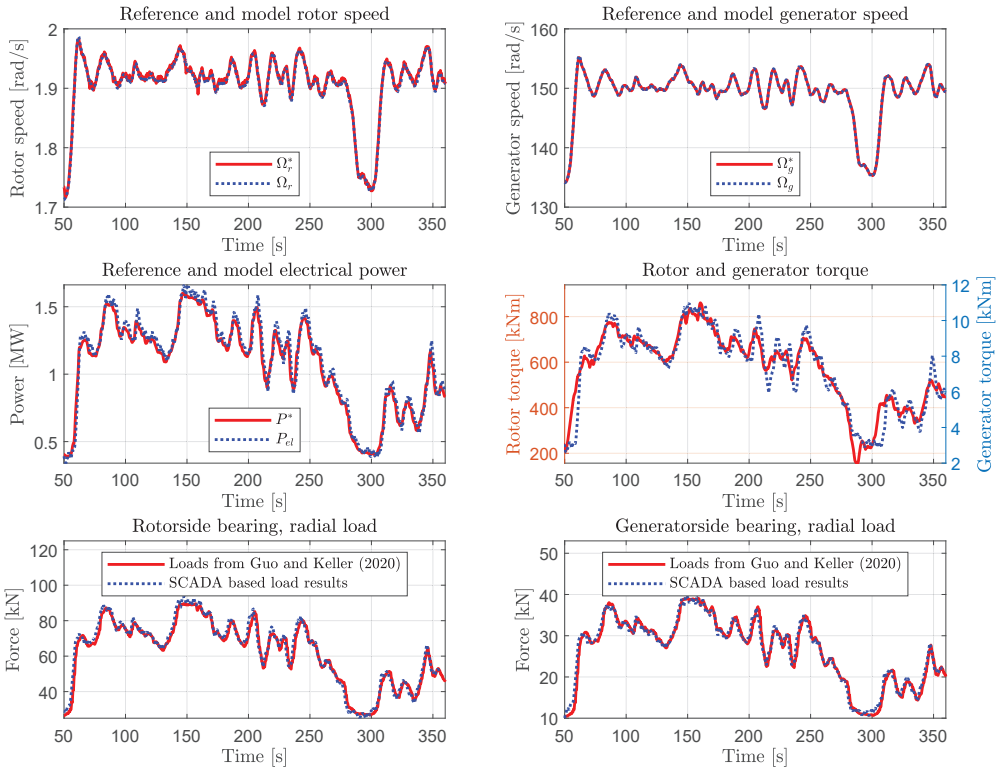

Figure 6. From top left to bottom right: Reference and model parameter comparison, rotor and generator torque comparison and radial bearing load comparison.

3.2. Accumulative damage

Bearing accumulative damage and expected lifetime is shown in Figure 7 for each bearing. It can be seen that for a decrease and increase in bearing load, the gradient of damage accumulation becomes concave and convex respectively. Furthermore, expected lifetime increases and decreases for a decrease and increase in mean damage accumulation respectively.

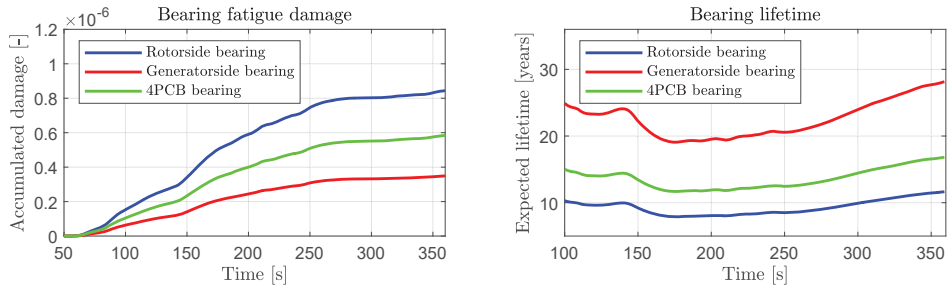

Figure 7. Bearing damage and total lifetime estimation for 90% reliability.

4. Concluding remarks and future work

A real-time physics-based model is developed using the bond graph approach. The model uses SCADA data with a sampling frequency of one hertz to impose a load reference on the wind turbine gearbox-generator model. Rotor torque is applied on the wind turbine hub, while generator speed is used as reference to the control loop for maximum power point tracking. The model is validated by comparing the rotor speed, generator speed and power production to the reference values of the model and by comparing the estimated bearing loads to Guo and Keller [20], where additional strain gauges are used for load estimation. The model can calculate expected lifetime on high-speed shaft bearings for high cycle fatigue.

Rotor torque can be determined from SCADA measurements when the rotor and generator inertia are known. The use of an incorrect rotor torque will significantly affect torsional results across the gearbox and the generator dynamics.

Bearing loads that support the high-speed shaft and pinion can be estimated from SCADA measurements without requiring additional sensors when operating between cut-in and cut-out wind speed. This does require additional knowledge on the dimensions of the shaft.

In the future, the model can be used in a digital twin framework, where system parameter estimation due to degradation can be included in combination with stochastic degradation models for future prognostics. The model can also be used for coupled fault sensitivity analysis between the drivetrain and the generator and can be further extended to other failure modes for gears, bearings, shafts and electrical components.

Acknowledgments

Thanks go to Jonathan Keller and Yi Guo for providing drivetrain properties and load results for this work.

References

[1] Stehly T, Beiter P and Duffy P 2020 *2019 Cost of Wind Energy Review* Tech. Rep. NREL/TP-5000-78471 National Renewable Energy Laboratory

[2] Faulstich S, Hahn B and Tavner P J 2011 *Wind Energy* **14** 327–337

[3] Nejad A R *et al.* 2022 *Wind Energy Science* **7** 387–411

[4] Tautz-Weinert J and Watson S J 2017 *Iet Renewable Power Generation* **11** 382–394

[5] Gray C S and Watson S J 2010 *Wind Energy* **13** 395–405

[6] Moghadam F K and Nejad A R 2022 *Mechanical Systems and Signal Processing* **162** 108087

[7] Tapia R and Medina A 2015 *Simulation Modelling Practice and Theory* **53** 149–166

[8] Khaouch Z *et al.* 2016 *ISA Transactions* **65** 418–436 ISSN 0019-0578

[9] Khaouch Z *et al.* 2017 *IOSR-JEEE* **12** 31–44 ISSN 2320-3331

[10] Gallego-Calderon J and Natarajan A 2015 *Engineering Structures* **103** 189–202

[11] Dong W, Xing Y and Moan T 2012 *Energies* **5** 4350–4371 ISSN 1996-1073

[12] Wang S, Nejad A R and Moan T 2020 *Wind Energy* **23** 1099–1117

[13] Remigius W D and Natarajan A 2021 *Wind Energy Science* **6** 1401–1412

[14] Helsen J 2021 *Acoustics Australia* **49** 251–258

[15] Liu Z and Zhang L 2020 *Measurement* **149** 107002 ISSN 0263-2241

[16] Karnopp D, Margolis D and Rosenberg R 2012 *System Dynamics: Modeling, Simulation, and Control of Mechatronic Systems: Fifth Edition* ISBN 9780470889084

[17] Niederstucke B *et al.* 2003 Load data analysis for wind turbine gearboxes Tech. rep.

[18] International Electrotechnical Commision (IEC) 2012 *Wind turbines - Part 4: Design requirements for wind turbine gearboxes* IEC61400–4:2012

[19] Palmgren A 1924 *Zeitschrift des Vereines Deutscher Ingenieure (ZVDI)* **14** 339–341

[20] Guo Y and Keller J 2020 *Tribology International* **148** 106347 ISSN 0301-679X

[21] Mathworks: Simulink - simulation and model-based design. URL `https://www.mathworks.com/products/simulink.html`

[22] van Binsbergen D, Nejad A R and Helsen J 2021 *Volume 9: Ocean Renewable Energy* V009T09A020

[23] Keller J and Lambert S 2019 *Gearbox Instrumentation for the Investigation of Bearing Axial Cracking* Tech. Rep. NREL/TP-5000-70639 National Renewable Energy Laboratory

[24] Keller J, Guo Y and Sethuraman L 2019 *Uptower Investigation of Main and High-Speed-Shaft Bearing Reliability* Tech. Rep. NREL/TP-5000-71529 National Renewable Energy Laboratory

[25] Santos R and van Dam J 2015 *Mechanical Loads Test Report for the U.S. Department of Energy 1.5-Megawatt Wind Turbine* Tech. Rep. NREL/TP-5000-63679 National Renewable Energy Laboratory

[26] Keller J 2020 DRC-uptower measurements, 2018-11-05: DRC15_fast_2018_11_05_20_47_58.h5

[27] 20sim: Software for modeling complex physics. URL `https://www.20sim.com/`

[28] Karnopp D, Margolis D and Rosenberg R 2012 *System Dynamics: Modeling, Simulation, and Control of Mechatronic Systems: Fifth Edition* pp 440–445 ISBN 9780470889084

[29] Pedersen E 2009 *Mathematical and Computer Modelling of Dynamical Systems* **15** 337–352

[30] Abad G *et al.* 2011 *Dynamic Modeling of the Doubly Fed Induction Machine* (John Wiley Sons, Ltd) ISBN 9781118104965

[31] Krause P *et al.* 2013 *Symmetrical Induction Machines* (John Wiley Sons, Ltd) ISBN 9781118524336

[32] Nesci Soares M 2022 *Multi-Physical Signal-and Model-Based Fault Detection, Isolation and Tolerance Technique for Power Electronic Converters in Wind Turbines* Ph.D. thesis Vrije Universiteit Brussel and Université Libre de Bruxelles, Engineering Sciences

[33] Akagi H, Watanabe E H and Aredes M 2017 *Instantaneous Power Theory and Applications to Power Conditioning* (John Wiley Sons) ISBN 9781119307181

[34] Kaura V and Blasko V 1997 *IEEE Transactions on Industry Applications* **33** 58–63

[35] Tripathi S M, Tiwari A N and Singh D 2016 *International Transactions on Electrical Energy Systems* **26** 1006–1031

[36] Frohr F and Orttenburger F 1982 *Introduction to Electronic Control Engineering* (Heyden) ISBN 0855012900

[37] Cohen S and Hindmarsh A C 1996 *Computers in Physics* **10** 138–143

[38] International Organization for Standardization (ISO) 2007 *Rolling bearings - Dynamic load ratings and rating life* ISO281:2007

[39] Nejad A R, Gao Z and Moan T 2014 *International Journal of Fatigue* **61** 116–128